

Tuning the superconducting transition of SrTiO₃-based 2DEGs with light

D. Arnold,¹ D. Fuchs,¹ K. Wolff,¹ and R. Schäfer¹*Institute for Solid-State Physics, Karlsruhe Institute of Technology, Karlsruhe, Germany*

(Dated: 8 April 2024)

The resistivity of the two dimensional electron gas that forms at the interface of strontium titanate with various oxides is sensitive to irradiation with visible light. In this letter we present data on the interface between the band gap insulators LaAlO₃ (LAO) and SrTiO₃ (STO). We operate a light emitting diode at temperatures below 1 K and utilize it to irradiate the LAO/STO interface at ultra low temperatures. On irradiation the resistance of this system is lowered continuously by a factor of five and the resistance change is persistent at low temperatures as long as the sample is kept in the dark. This makes a characterization of transport properties in different resistive states over extended time periods possible. Our pristine sample gets superconducting below 265 mK. The transition temperature T_c shifts downwards on the persistent photo-induced lowering of the resistance. The persistent photoconductance can be completely reverted by heating the structure above 10 K in which case T_c as well takes on its original value. Thus very similar to field effect control of electron densities irradiation at low temperatures offers a versatile tuning knob for the superconducting state of STO-based interfaces which in addition has the advantage to be nonvolatile.

A two dimensional electron gas (2DEG) develops at the interface between strontium titanate (STO) and a variety of different oxides^{1–11} which offers a huge playground for many kind of solid state phenomena (e.g. Ref. 12). Here we focus on low temperature transport properties which are known to be sensitive to exposure of the 2DEG to visible light at room temperature.^{13–16} Careful experiments keep therefore all samples for a considerable time in a dark environment (typically 24 h) prior to cool down to avoid photo-induced effects which otherwise lead to relaxation effects and a drift of transport coefficients on amazingly long time scales.¹³ The effect of photo induced conductivity has of course been addressed as an independent subject of interest.^{17–19} It has been studied in recent years from room temperature down to $T = 1.5$ K and was found to be persistent at low temperature¹⁸ in accordance with the aforementioned precautions taken by many researchers. The persistent charge carriers have been linked to oxygen vacancies trapped at domain boundaries which develop below the so-called antiferrodistortive transition at 105 K.¹⁹

A salient feature of low temperature transport of STO-based 2DEGs is superconductivity found below $T = 300$ mK.^{20–22} The two dimensional confinement of the mobile carriers make it easy to gate tune its density and in turn the conductance by the field effect.²³ For the superconducting transition temperature T_c a dome shaped structure in the phase diagram^{24,25} was found, which resembles celebrated findings in the cuprates and bulk STO. However, despite a decade of intense research the microscopic origin of the shift in T_c with gate tuning remains controversial, as the influence and interplay of important parameters like disorder, inhomogeneity and spin-orbit coupling is not fully understood. It is therefore desirable to find new control parameters altering transport characteristics.²⁶

In this letter we establish persistent photo-conductance as another tuning knob for the superconducting transition temperature which might give further insight in the nature of the superconducting state of the STO-based 2DEG. We operate a light emitting diode (LED) at dilution fridge temperatures. By stabilizing the temperature at $T = 500$ mK we can monitor the resistance during irradiation by the LED and find a continu-

ous reduction. When the LED is switched off the resistance is constant. On the time scale of our experiment (which in some cases extended for a period of more than a week) we could not detect any change of resistance as long as the temperature stays well below $T < 1$ K and the LED is switched off. However, the resistance change can be completely reverted by a controlled elevation of temperature to $1 \text{ K} < T < 15 \text{ K}$. The phenomenon seems to be a rather general feature and has so far been observed in LaAlO₃/SrTiO₃ (LAO/STO) heterostructures as well as in the γ -Al₂O₃/SrTiO₃ system. Here we present exemplary data on a LAO/STO sample where we could reduce the resistance by a factor of five. The rate of resistance change depends on the radiant flux of the LED and is to first order proportional to the LED current. Adjusting the radiant energy we can set the resistance value within the total tuning range on purpose. This statement is true for both directions of resistance change. Resistance can be tuned downwards by light and upwards again by elevation of temperature.

The sample has been prepared by standard pulsed laser ablation using TiO₂-terminated (001) SrTiO₃ substrates and LaAlO₃ single crystal targets. Film deposition was done at an oxygen partial pressure of $p(\text{O}_2) = 10^{-5}$ mbar onto a substrate heated to $T_{\text{sub}} = 700^\circ\text{C}$. More details on sample preparation and patterning are described elsewhere.^{27,28} Electrical connections to the six arms of a Hall bar geometry are made by ultrasound wire bonding with aluminum leads.

For the purpose of irradiating the Hall bar structure at $T < 1$ K we use a white LED (OSRAM "Golden DRAGON Plus", type LW W5AM)²⁹ with a radiation spectrum made up of a narrow primary emission line centered around a wavelength of 460 nm and a broad photo luminescence (PL) band with a maximal intensity around 565 nm. The diode is intended to be used in the temperature range $-40^\circ\text{C} < T < 125^\circ\text{C}$.²⁹ By recording I/U characteristics in an extended temperature range (Fig. 1 (a)) we gained confidence that the LED works properly even below $T < 1$ K. As expected, the forward voltage shifts to higher voltages on cool down but this shift is rather moderate. At $T = 77$ K we could operate the LED in an open dewar and check by visual inspection that the emitted light did not show a noticeable shift in color. However, to avoid excess heating

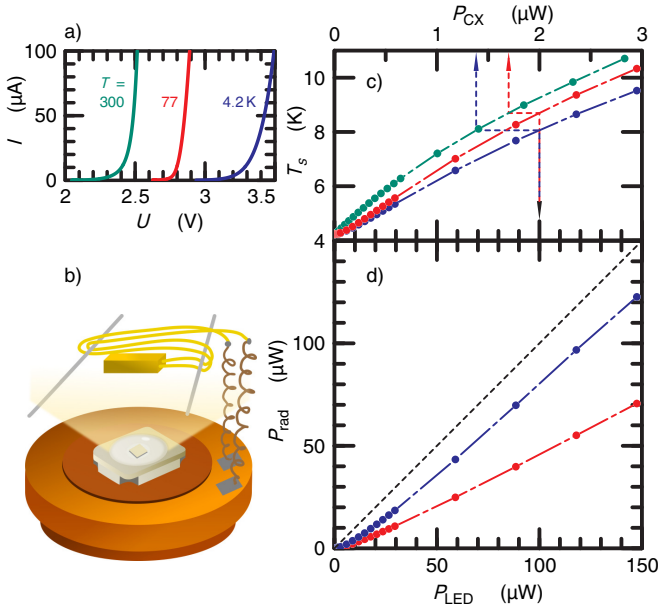


FIG. 1. (a) I/U characteristics of the light emitting diode (LED) at different temperatures. (b) Schematics of the LED calibration experiment. The radiant flux of the LED irradiates a thermometer chip (gold) supported by thin nylon fibres (gray). The leads for measuring the thermometer resistance consist of thin manganin wires. (c) Temperature of the thermometer chip as a function of electrical power dissipated by the LED (lower scale labeled P_{LED} , red and blue data). In the same diagram the temperature elevation due to self heating of the thermometer (upper scale labeled P_{CX} , green data) is shown. With the help of this diagram P_{LED} can be mapped onto the power dissipated by thermometer due to light absorption. The difference between the red and the blue data is explained in the text. (d) Radiant flux of the LED as a function of effective input power at $T = 4.2$ K. The data shown in blue represent the total flux, while data shown in red correspond to the part of the spectrum absorbed by a gold plated surface.

when used at $T < 1$ K the LED has to be operated at extremely low currents (below $I_{LED} < I_{max} = 50 \mu A$), owing to the limited cooling power of our dilution fridge. I_{max} is by more than three orders of magnitude smaller than the minimal recommended diode current 100 mA.²⁹ It is not clear how efficient electrical power is converted into electromagnetic radiation in this situation.

To gain some knowledge of the efficiency we performed the experiment sketched in Fig. 1 (b) in which the LED is held at $T = 4.2$ K and a resistive thermometer is mounted at a distance of 10 mm with sufficient thermal resistance to show a well resolved temperature rise when irradiated at low diode currents. The setup is installed on a general purpose puck of a physical property measurement system (PPMS, Quantum Design) which provides the temperature reservoir. The LED is thermally anchored thoroughly to the puck while the calibrated Cernox thermometer (R_{CX}) (Lake Shore Cryotronics, CX-1050-SD-1.4L) is supported by two thin Nylon fibers (80 μm diameter, actually dominating the thermal resistance) and electrically connected by two 30 μm thick Manganin wires of about 150 mm length. When irradiated by the

LED or self-heated by a sufficiently high measurement current I_{CX} the thermometer reaches an elevated steady state temperature T_s after a relaxation time of typically 30 min. We measure T_s as a function of I_{CX} and the diode current I_{LED} . A rise of T_s as response to a diode current is clear evidence for the presence of an irradiance flux absorbed by R_{CX} . We take the smallest forward voltage $U_{LED} = 2.95$ V at which we could observe a temperature rise in R_{CX} (corresponding to a diode current $I_{LED} = 100$ nA) as a measure of the photon energy of the primary emission line at $T = 4.2$ K. The radiant energy of the LED is then strictly bounded by the effective power $P_{LED} = I_{LED} \cdot 2.95$ V. In Fig. 1 (c) we display T_s as function of P_{LED} for two different runs. The blue data are recorded while the thermometer chip had its original gold plated color. It then absorbs predominantly the short wavelength photons from the main emission line while the longer wavelength PL photons are reflected. In a first run (red) the thermometer chip was covered by a black paint produced by mixing varnish (GE 7031) with carbon black. In this case the absorption includes the long wavelength part of the spectrum resulting in an increased T_s at identical P_{LED} levels. We also recorded T_s as a function of the dissipated power P_{CX} due to self heating when I_{CX} is increased giving identical results in both runs (green). As indicated by the arrow headed lines in Fig. 1 (c), we can relate P_{LED} to P_{CX} which gives a measure for the irradiance flux absorbed by R_{CX} . Finally, a geometry factor f can be deduced relating radiant power of the LED to irradiance flux received by the surface of R_{CX} . Actually, uncertainties in the latter quantity dominates the systematic error of this experiment and limits the accuracy of the final result presented in Fig. 1 (d) to about 20%. In this figure f is taken into account to calculate the radiant flux P_{rad} which is plotted as a function of P_{LED} . The black dashed line represents the theoretical limit, while the blue and red data represent the fraction of radiant flux dissipated by a black and gold plated absorber, respectively. Fig. 1 (d) reports an amazingly high efficiency of the LED at 4.2 K. The total radiant intensity of our light source is about $500 \text{ nW}/(\mu A \text{ sr}) \cdot I_{LED}$ in forward direction. The persistent photoconductance discussed in the rest of this letter is most likely caused by the short wave length part of the spectrum (this is the radiation absorbed by the gold plated R_{CX}). Its radiant intensity is found to be $300 \text{ nW}/(\mu A \text{ sr}) \cdot I_{LED}$.

After characterizing the light source, we describe in the rest of this letter our main experiment sketched in Fig. 2 (a) which is installed in a commercial dilution refrigerator (Oxford Instruments, MX250). The Hall bar structured sample is thermally anchored at a sample stage. The temperature of the sample stage T_{ss} is PID regulated using a resistor chip R_h as heater and can be controlled in the range $12 \text{ mK} < T_{ss} < 2$ K. Reaching higher temperatures is difficult without removing the $^3\text{He}/^4\text{He}$ insert from the liquid helium bath. Nevertheless, we managed to heat our sample to about $T_{ss} \approx 10$ K by running our insert in a special operation mode (see below). In this case the temperature is only weakly controlled. The sheet resistance R_{\square} of the sample is measured with a lock-in technique: An ac current of amplitude $I_{AC} = 9$ nA which is reduced to $I_{AC} = 2$ nA for temperature dependent $R_{\square}(T)$ measurements is sourced to the central strip of the Hall bar structure. The

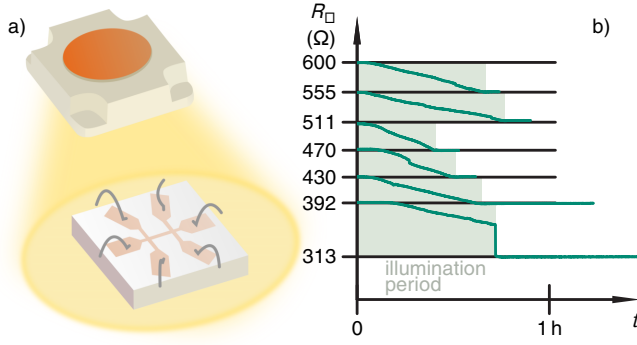


FIG. 2. (a) Schematics of the LAO/STO sample structured in Hall bar geometry and irradiated by a LED. The setup is operated in a dilution refrigerator at $T \leq 500$ mK. (b) Sheet resistance R_{\square} vs. time at $T = 500$ mK. During light exposure (period marked in green) R_{\square} drops continuously while it stays constant when the LED is switched off. In some instances R_{\square} display a sudden jump during illumination. One such instance can be seen between 392 Ω and 313 Ω .

resulting voltage drop U_{AC} over two side terminals is amplified by a home-build amplifier and measured by the lock-in amplifier (Signal Recovery, Model 7265 DSP). The length between the voltage terminals equals 12 times the width of the central strip and $R_{\square} = U_{AC}/(12I_{AC})$. We carefully checked that we stay in the linear regime of the current voltage characteristics which made it necessary to reduce the measurement current close the superconducting transition. Hall resistance is recorded in fields up to 8 T by measuring the voltage across two terminals opposite to each other and supplies us with information on the sheet carrier concentration.

The LED light source is mounted at ~ 10 mm distance from the sample. LED currents of $100 \text{ nA} < I_{LED} < 50 \mu\text{A}$ are supplied by a source/measure unit (Keithley Model 2400) via superconducting leads. Operating the LED at higher power leads to a heat burden of the sample stage. In principle I_{LED} could replace the current sourced to R_h in the PID regulation circuit. For the experiments described here we use R_h for temperature control and always stabilize the stage at $T_{ss} = 500$ mK before slowly turning on I_{LED} . The PID regulation reacts to increasing P_{LED} by reducing the current sourced to R_h keeping T_{ss} almost constant ($|\Delta T_{ss}| < 5$ mK). At $I_{LED} = 50 \mu\text{A}$ the current through R_h is set to zero by the PID circuitry and heating is solely due to the dissipation of the LED.

Constant T_{ss} does not automatically guarantee a constant temperature of the 2DEG at the LAO/STO interface of our sample. Because of the positive temperature coefficient of R_{\square} at $T = 500$ mK, an increase of temperature of the 2DEG as response to irradiation would result in an increase of R_{\square} . In the contrary, light exposure at constant T_{ss} leads to a decrease of R_{\square} . It alters the resistive state of our sample and this alteration cannot be attributed to heating. Examples are given in in Fig. 2 (b). Within the green marked period the sample was illuminated by setting I_{LED} to values between 1 and $5 \mu\text{A}$. During illumination R_{\square} decreases as a function of time. As soon as we turn off I_{LED} , R_{\square} stabilizes at its reduced, momentary value. As long as the LED remains switched off and $T_{ss} \lesssim 1$ K,

R_{\square} is a function of magnetic field and temperature only and does not change over time. Initially, $R_{res} \equiv R_{\square}(T = 500 \text{ mK})$ was found to be $R_{res} = 600 \Omega$. Subsequently we altered the resistive state of our sample in steps of about 42 Ω . In Fig. 3 (a) where R_{res} is displayed as a function of the radiant exposure D , this first series is represented by red symbols. The abscissa in this figure is deduced from $\int I_{LED} dt$ with the help of the LED calibration presented earlier and corresponds to the total radiant energy per unit area irradiated to the sample by the LED in the short wavelength part of the spectrum. Most likely only high energetic photons are responsible for the persistent conductance effect.¹⁹ However, we do not have further evidence for this statement and additional experiments with monochromatic LEDs are required for a proof. The total radiant exposure over all wavelength is 70% larger.

Light exposure leads to persistent reduction of R_{\square} . However, the resistance change can be reverted by heating the sample to $T_{ss} > 1$ K. The rate of resistance *increase* depends in this case on temperature and speeds up considerable above $T > 4.2$ K. Unfortunately it is almost impossible to regulate temperatures in the regime $T > 2$ K in our dilution fridge. While we could reach temperatures of the order $12 \text{ K} > T > 10 \text{ K}$ by thermally isolating³⁰ and heating the mixing chamber this temperature is only weakly controlled. Nevertheless, we could convince ourselves, that R_{res} measured after cooling the sample down again after heat treatment depends strongly on the peak temperature reached during the procedure and only weakly on the time period it lasts. The minimal resistance $R_{res} = 120 \Omega$ we could achieve by irradiation is in this respect related to the temperature $T = 500$ mK at which it is measured and lower resistive states might in principle be reached by irradiation at lower temperatures but relax back to $R_{res} = 120 \Omega$ if the sample is heated to $T = 500$ mK.

By controlled heating we are able to increase R_{res} in small steps. Again, at low temperature and while the LED is switched off, R_{\square} is a function of magnetic field and temperature only and is absolutely stable over time. By heating the sample to $T_{ss} \approx 12$ K we could reach resistance states with even slightly higher $R_{res} = 675 \Omega$ than the initial value of 600 Ω . Subsequently we lowered the resistance again by utilizing the LED. This second run is shown as green symbols in Fig. 3 (a) giving consistent results. Analyzing the dependence of $R_{res}(D)$ gives the empirical results shown as black lines in Fig. 3 (a). The experimental data are well described by

$$R_{res}(D) = R_{ini} - \Delta R \cdot L_D, \quad L_D \equiv 10 \log_{10} \left(\frac{D}{1 (\text{mJ cm}^{-2})} \right) \text{ dB},$$

with different initial resistance values ($R_{ini} = 617 \Omega, 215 \Omega$) and slopes ($\Delta R = 26.5 \Omega/\text{dB}, 2.65 \Omega/\text{dB}$) at lower and higher dose, respectively.

In Fig. 3 (b) we present $R_{\square}(T)$ in the different persistent resistance states of the first light induced reduction series (corresponding to the red symbols in Fig. 3 (a)). During this measurements $I_{LED} = 0$. The curves in Fig. 3 (b) display superconductivity at low temperatures with a transition temperature T_c which shifts downwards with decreasing R_{res} . This effect is summarized in Fig. 3 (c) where T_c was estimated as the temperature where $R_{\square}(T_c) = R_{res}/2$. In the initial sequence

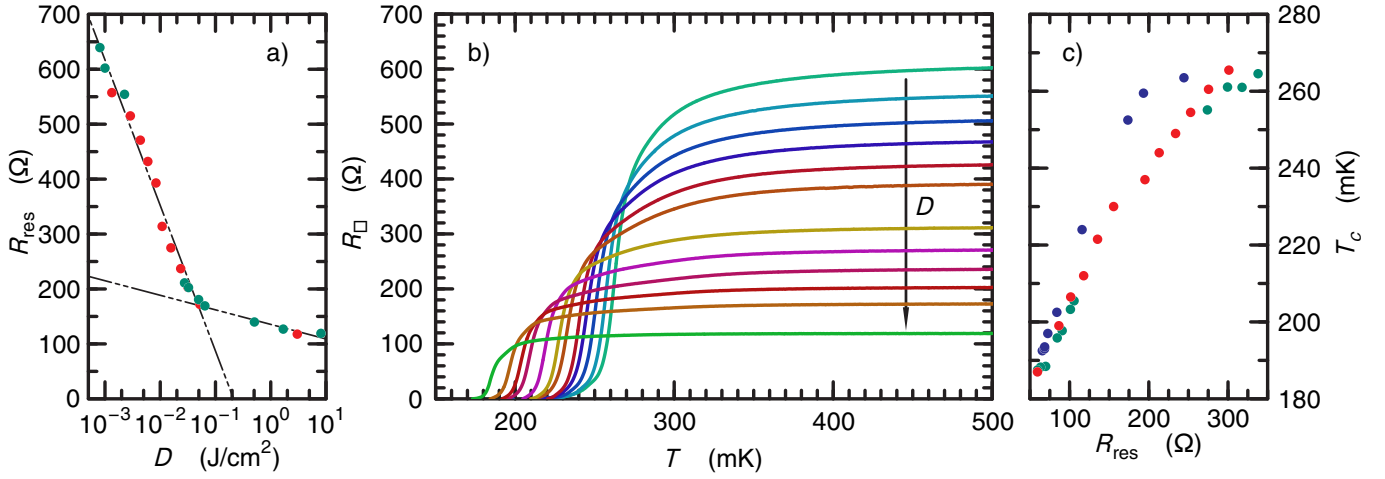


FIG. 3. (a) Residual sheet resistance $R_{\text{res}} = R_{\square}(500 \text{ mK})$ as function of radiant exposure D in the short wavelength part of the LED spectrum. Red dots correspond to the irradiance sequence shown in (b). Green dots represent the result of a second sequence recorded after a temperature induced reset of R_{res} . Black lines are guide to the eyes explained further in the text. (b) Sheet resistance R_{\square} as a function of temperature T for various residual resistances R_{res} . The shown curves are measured successively while R_{res} has been reduced in between by a controlled irradiation. The LED is off during the measurements. (c) Superconducting transition temperature T_c as function of R_{res} . Red and green symbols as in (a), while blue dots are results during temperature controlled resistance increase.

of resistance reduction by illumination T_c decreased monotonically from $T_c = 265 \text{ mK}$ down to $T_c = 187 \text{ mK}$. The blue symbols represent the findings when R_{res} recovers due to controlled heating. $R_{\text{res}} = 490 \Omega$ could be reached easily by heating the sample to $T \approx 11 \text{ K}$. In this state T_c fully recovers to $T_c = 264 \text{ mK}$. We then kept the sample for an extended period of several days at $T \lesssim 12 \text{ K}$ and could increase R_{res} even further ($R_{\text{res}} = 675 \Omega$). However, this had only a minor effect on T_c . The final illumination sequence with falling R_{res} is shown as green symbols and shows the reproducibility of our finding.

The observed reduction of T_c with decreasing R_{res} is typical for the so called over-doped regime and indeed taking the resistance range of our experiment ($120 \Omega < R_{\square} < 600 \Omega$) into account this finding is in accord with published data^{24,25} on field effect tuned resistivities. Our Hall resistivity measurements show a zero field slope ($R_H = 43 \Omega/\text{T}$) which is almost independent of R_{res} in accordance with data presented in Ref. 31. Within the limited field range of our magnet ($\pm 8 \text{ T}$) we only see slight nonlinearities at larger fields which get more pronounced as R_{res} is lowered. This trend has already been reported previously for LAO/STO in the over-doped regime.

For now, the microscopic mechanism of light induced changes is absolutely unclear. Findings by other authors¹⁹ differ in subtle details. We completely revert the photo-induced transport changes at comparatively low temperatures ($T \approx 12 \text{ K}$) while in Ref. 19 a crossing of the antiferro-distortive transition of STO at $T \approx 105 \text{ K}$ seems to be necessary to revert persistence in photo-conductance. The difference might route in a smaller photon energy in our case. The LED radiates at $h\nu \lesssim 2.95 \text{ eV}$, which is of the order but considerable smaller than the band gap of STO ($E_{\text{gap}} = 3.2 \text{ eV}$). Other experiments on persistent photo-conductance use UV light above the gap energy.

In summary, we present a setup to tune the transport behavior of STO-based interfaces at low temperatures with light. The radiant intensity of a LED was calibrated at $T = 4.2 \text{ K}$ as a function of current and utilized as the light source below 1 K . Adjusting the radiant energy we were able to tune the residual sheet resistance R_{res} at 500 mK , while simultaneously changing the superconducting transition temperature T_c . We reported a monotonous behavior of T_c vs R_{res} for different resistive states. To reverse the altered state we used heat treatment up to 12 K . Using visible light at low temperatures we are introducing a new nonvolatile tuning parameter on the superconductivity of the STO-based interfaces.

This paper was supported by the Deutsche Forschungsgemeinschaft (Grant SCHA 658/2-1 and FU 457/2-1). We thank K. Grube for fruitful discussion.

¹A. Ohtomo and H. Y. Hwang, "A high-mobility electron gas at the LaAlO₃/SrTiO₃ heterointerface," *Nature* **427**, 423–426 (2004).

²S. S. A. Seo, W. S. Choi, H. N. Lee, L. Yu, K. W. Kim, C. Bernhard, and T. W. Noh, "Optical study of the free-carrier response of LaTiO₃/SrTiO₃ superlattices," *Phys. Rev. Lett.* **99**, 266801 (2007).

³P. Perna, D. Maccariello, M. Radovic, U. Scotti di Uccio, I. Pallecchi, M. Codda, D. Marré, C. Cantoni, J. Gazquez, M. Varela, S. J. Pennycook, and F. M. Granozio, "Conducting interfaces between band insulating oxides: The LaGaO₃/SrTiO₃ heterostructure," *Applied Physics Letters* **97**, 152111 (2010), <https://doi.org/10.1063/1.3496440>.

⁴P. Moetakef, T. A. Cain, D. G. Ouellette, J. Y. Zhang, D. O. Klenov, A. Janotti, C. G. Van de Walle, S. Rajan, S. J. Allen, and S. Stemmer, "Electrostatic carrier doping of GdTiO₃/SrTiO₃ interfaces," *Applied Physics Letters* **99**, 232116 (2011), <https://doi.org/10.1063/1.3669402>.

⁵D. F. Li, Y. Wang, and J. Y. Dai, "Tunable electronic transport properties of DyScO₃/SrTiO₃ polar heterointerface," *Applied Physics Letters* **98**, 122108 (2011), <https://doi.org/10.1063/1.3570694>.

⁶S. W. Lee, Y. Liu, J. Heo, and R. G. Gordon, "Creation and control of two-dimensional electron gas using Al-based amorphous oxides/SrTiO₃ heterostructures grown by atomic layer deposition," *Nano Letters* **12**, 4775–4783 (2012), <https://doi.org/10.1021/nl302214x>.

⁷C. He, T. D. Sanders, M. T. Gray, F. J. Wong, V. V. Mehta, and Y. Suzuki,

- “Metal-insulator transitions in epitaxial LaVO₃ and LaTiO₃ films,” *Phys. Rev. B* **86**, 081401 (2012).
- ⁸A. Annadi, A. Putra, Z. Q. Liu, X. Wang, K. Gopinadhan, Z. Huang, S. Dhar, T. Venkatesan, and Ariando, “Electronic correlation and strain effects at the interfaces between polar and nonpolar complex oxides,” *Phys. Rev. B* **86**, 085450 (2012).
- ⁹C. Li, Q. Xu, Z. Wen, S. Zhang, A. Li, and D. Wu, “The metallic interface between insulating NdGaO₃ and SrTiO₃ perovskites,” *Applied Physics Letters* **103**, 201602 (2013), <https://doi.org/10.1063/1.4830042>.
- ¹⁰Y. Z. Chen, N. Bovet, F. Trier, D. V. Christensen, F. M. Qu, N. H. Andersen, T. Kasama, W. Zhang, R. Giraudo, J. Dufouleur, T. S. Jespersen, J. R. Sun, A. Smith, J. Nygård, L. Lu, B. Büchner, B. G. Shen, S. Linderoth, and N. Pryds, “A high-mobility two-dimensional electron gas at the spinel/perovskite interface of γ -Al₂O₃/SrTiO₃,” *Nature Communications* **4**, 1371 (2013).
- ¹¹P. Xu, D. Phelan, J. Seok Jeong, K. Andre Mkhoyan, and B. Jalan, “Stoichiometry-driven metal-to-insulator transition in NdTiO₃/SrTiO₃ heterostructures,” *Applied Physics Letters* **104**, 082109 (2014), <https://doi.org/10.1063/1.4866867>.
- ¹²P. Zubko, S. Gariglio, M. Gabay, P. Ghosez, and J.-M. Triscone, “Interface physics in complex oxide heterostructures,” *Annual Review of Condensed Matter Physics* **2**, 141–165 (2011), <https://doi.org/10.1146/annurev-conmatphys-062910-140445>.
- ¹³M. Huijben, G. Rijnders, D. H. A. Blank, S. Bals, S. V. Aert, J. Verbeeck, G. V. Tendeloo, A. Brinkman, and H. Hilgenkamp, “Electronically coupled complementary interfaces between perovskite band insulators,” *Nature Materials* **5**, 556–560 (2006).
- ¹⁴Y. Lei, Y. Li, Y. Z. Chen, Y. W. Xie, Y. S. Chen, S. H. Wang, J. Wang, B. G. Shen, N. Pryds, H. Y. Hwang, and J. R. Sun, “Visible-light-enhanced gating effect at the LaAlO₃/SrTiO₃ interface,” *Nature Communications* **5**, 5554 (2014).
- ¹⁵Y. Li, Y. Lei, B. G. Shen, and J. R. Sun, “Visible-light-accelerated oxygen vacancy migration in strontium titanate,” *Scientific Reports* **5**, 14576 (2015).
- ¹⁶A. Tebano, E. Fabbri, D. Pergolesi, G. Balestrino, and E. Traversa, “Room-temperature giant persistent photoconductivity in SrTiO₃/LaAlO₃ heterostructures,” *ACS Nano* **6**, 1278–1283 (2012), <https://doi.org/10.1021/nn203991q>.
- ¹⁷Z. Yang, Y. Chen, H. Zhang, H. Huang, S. Wang, S. Wang, B. Shen, and J. Sun, “Joint effect of gate bias and light illumination on metallic LaAlO₃/SrTiO₃ interface,” *Applied Physics Letters* **111**, 231602 (2017), <https://doi.org/10.1063/1.5009790>.
- ¹⁸L. Cheng, L. Wei, H. Liang, Y. Yan, G. Cheng, M. Lv, T. Lin, T. Kang, G. Yu, J. Chu, Z. Zhang, and C. Zeng, “Optical manipulation of rashba spin-orbit coupling at SrTiO₃-based oxide interfaces,” *Nano Letters* **17**, 6534–6539 (2017), <https://doi.org/10.1021/acs.nanolett.7b02128>.
- ¹⁹M. Yazdi-Rizi, P. Marsik, B. P. P. Mallett, K. Sen, A. Cerreta, A. Dubroka, M. Scigaj, F. Sánchez, G. Herranz, and C. Bernhard, “Infrared ellipsometry study of photogenerated charge carriers at the (001) and (110) surfaces of SrTiO₃ crystals and at the interface of the corresponding LaAlO₃/SrTiO₃ heterostructures,” *Phys. Rev. B* **95**, 195107 (2017).
- ²⁰N. Reyren, S. Thiel, A. D. Caviglia, L. F. Kourkoutis, G. Hammerl, C. Richter, C. W. Schneider, T. Kopp, A.-S. Rüetschi, D. Jaccard, M. Gabay, D. A. Müller, J.-M. Triscone, and J. Mannhart, “Superconducting interfaces between insulating oxides,” *Science* **317**, 1196–1199 (2007), <https://science.sciencemag.org/content/317/5842/1196.full.pdf>.
- ²¹J. Biscaras, N. Bergeal, A. Kushwaha, T. Wolf, A. Rastogi, R. C. Budhani, and J. Lesueur, “Two-dimensional superconductivity at a mott insulator/band insulator interface LaTiO₃/SrTiO₃,” *Nature Communications* **1**, 89 (2010).
- ²²D. Fuchs, R. Schäfer, A. Sleem, R. Schneider, R. Thelen, and H. von Löhneysen, “Two-dimensional superconductivity between SrTiO₃ and amorphous Al₂O₃,” *Applied Physics Letters* **105**, 092602 (2014), <https://doi.org/10.1063/1.4895120>.
- ²³S. Thiel, G. Hammerl, A. Schmehl, C. W. Schneider, and J. Mannhart, “Tunable quasi-two-dimensional electron gases in oxide heterostructures,” *Science* **313**, 1942–1945 (2006), <https://science.sciencemag.org/content/313/5795/1942.full.pdf>.
- ²⁴A. D. Caviglia, S. Gariglio, N. Reyren, D. Jaccard, T. Schneider, M. Gabay, S. Thiel, G. Hammerl, J. Mannhart, and J.-M. Triscone, “Electric field control of the LaAlO₃/SrTiO₃ interface ground state,” *Nature* **456**, 624–627 (2008).
- ²⁵S. Gariglio, M. Gabay, and J.-M. Triscone, “Research update: Conductivity and beyond at the LaAlO₃/SrTiO₃ interface,” *APL Materials* **4**, 060701 (2016), <https://doi.org/10.1063/1.4953822>.
- ²⁶D. Fuchs, A. Sleem, R. Schäfer, A. G. Zaitsev, M. Meffert, D. Gerthsen, R. Schneider, and H. v. Löhneysen, “Incipient localization of charge carriers in the two-dimensional electron system in LaAlO₃/SrTiO₃ under hydrostatic pressure,” *Phys. Rev. B* **92**, 155313 (2015).
- ²⁷D. Fuchs, K. Wolff, R. Schäfer, R. Thelen, M. Le Tacon, and R. Schneider, “Patterning of two-dimensional electron systems in SrTiO₃ based heterostructures using a CeO₂ template,” *AIP Advances* **7**, 056410 (2017), <https://doi.org/10.1063/1.4973696>.
- ²⁸K. Wolff, R. Eder, R. Schäfer, R. Schneider, and D. Fuchs, “Anisotropic electronic transport and rashba effect of the two-dimensional electron system in (110) SrTiO₃-based heterostructures,” *Phys. Rev. B* **98**, 125122 (2018).
- ²⁹*Golden DRAGON Plus*, Osram Opto Semiconductors GmbH (2010).
- ³⁰This is done by pumping out the ³He/⁴He-mixture. An absorption pump at the condenser is still kept at $T = 1.7$ K to maintain good isolation from the ⁴He bath. This, actually, limits the maximal sample temperature we can reach by heating the mixing chamber.
- ³¹A. Joshua, S. Pecker, J. Ruhman, E. Altman, and S. Ilani, “A universal critical density underlying the physics of electrons at the LaAlO₃/SrTiO₃ interface,” *Nature Communications* **3**, 1129 (2012).